AD 728406

UNCLASSIFIED
Security Classification

DOCUMENT CONTROL DATA - R & D

(Security classification of title, body of abstract and indexing annotation must be entered when the overall report is classified)

1. ORIGINATING ACTIVITY (Corporate author)	2a. REPORT SECURITY CLASSIFICATION
Naval Ship Research and Development Center Washington, D. C. 20034	UNCLASSIFIED
	2b. GROUP

3. REPORT TITLE

HYDROFOIL FLUTTER ANALYSIS, USING A MODIFIED STRIP THEORY

4. DESCRIPTIVE NOTES (Type of report and inclusive dates)
Final Report

5. AUTHOR(S) (First name, middle initial, last name)

Yuan-Ning Liu and Peter K. Besch

6. REPORT DATE	7a. TOTAL NO. OF PAGES	7b. NO. OF REFS
July 1971	56	19

8a. CONTRACT OR GRANT NO.	9a. ORIGINATOR'S REPORT NUMBER(S)
b. PROJECT NO. Subproject S4606	3624
c. Task 1703	9b. OTHER REPORT NO(S) (Any other numbers that may be assigned this report)
d.	

10. DISTRIBUTION STATEMENT

APPROVED FOR PUBLIC RELEASE: DISTRIBUTION UNLIMITED

11. SUPPLEMENTARY NOTES	12. SPONSORING MILITARY ACTIVITY
	Naval Ship Systems Command

13. ABSTRACT

A flutter theory based on modified Yates hydrodynamic loading was used to predict the flutter characteristics of five hydrofoil flutter models. Theoretical flutter speeds were unconservative when flutter was predicted to occur in a predominantly bending mode, and conservative when flutter was predicted to occur in a predominantly torsional mode. The theory may be useful for hydrofoils which are susceptible to flutter in a torsional mode.

DD FORM 1 NOV 65 1473 (PAGE 1)

S/N 0101-807-6801

UNCLASSIFIED
Security Classification

14 KEY WORDS	LINK A		LINK B		LINK C	
	ROLE	WT	ROLE	WT	ROLE	WT
Aspect ratio						
Mass ratio						
Hydrofoil						
Flutter						
Hydroelasticity						

DEPARTMENT OF THE NAVY
NAVAL SHIP RESEARCH AND DEVELOPMENT CENTER
WASHINGTON, D. C. 20034

HYDROFOIL FLUTTER ANALYSIS, USING A MODIFIED STRIP THEORY

by

Yuan-Ning Liu and Peter K. Besch

July 1971

Report 3624

TABLE OF CONTENTS

LIST OF FIGURES

LIST OF TABLES

NOTATION

Symbol	Definition
AR	Aspect ratio; square of distance from root position to tip of hydrofoil divided by one-half the area of hydrofoil from root to tip
A*	Local aspect ratio; square of distance from local position to tip of hydrofoil divided by one-half the area of hydrofoil from local position to tip of hydrofoil
a	Nondimensional distance from midchord to elastic axis, measured perpendicular to elastic axis, positive rearward as fraction of semichord b
a_c	Nondimensional distance from midchord to local aerodynamic center (for steady flow) measured perpendicular to elastic axis, positive rearward as fraction of semichord b
b	Semichord of hydrofoil measured perpendicular to elastic axis
[C]	Damping matrix of the structure
[C*]	Hydrodynamic damping matrix with complex elements
C(k)	Complex Theodorsen circulation function
$C_{\ell\alpha}$	Local lift slope for a hydrofoil section perpendicular to elastic axis in steady flow
EI	Bending stiffness
$\{F_i\}$	Unsteady hydrodynamic forces
GJ	Torsional stiffness
g	Structural damping coefficient; also, gravitational acceleration
H	Amplitude of oscillation of h
h	Local vertical translational displacement of hydrofoil at elastic axis, positive upward
Im(s)	Imaginary part of s
I_α	Mass moment of inertia per unit span about elastic axis
j	$\sqrt{-1}$
[K]	Stiffness matrix of the structure
[K*]	Hydrodynamic stiffness matrix with complex elements
k	Reduced frequency $b\omega/V$
L	Length of semispan measured along elastic axis
ℓ	Distance from free surface to tip of hydrofoil

Symbol	Definition
M	Oscillatory moment about elastic axis per unit span of hydrofoil, positive leading edge up
$[M]$	Mass matrix of the structure
$[M^*]$	Virtual mass matrix
m	Mass per unit span along elastic axis
P	Oscillatory lift per unit span of hydrofoil along elastic axis, positive upward
p	Spanwise modification factor for noncirculatory loading
$Re(s)$	Real part of s
r_α	Nondimensional radius of gyration $\sqrt{I_\alpha/mb^2}$
s	Complex eigenvalue
t	Time
V	Flow speed
x	Translational displacement perpendicular to hydrofoil
x_α	Nondimensional distance from elastic axis to center of gravity, measured perpendicular to elastic axis, positive aft as fraction of semichord b
y	Spanwise coordinate along elastic axis of hydrofoil
w	Downwash; vertical component of flow velocity on foil, positive downward
δ	Exponential decay factor, corresponding to oscillation of amplitude proportional to $e^{-\delta t}$
ζ	Damping factor δ/ω
Θ	Amplitude of oscillation of θ
θ	Local torsional displacement of hydrofoil measured about elastic axis, positive leading edge up
Λea	Elastic-axis sweep angle, positive for sweepback
μ	Mass ratio $m/\pi\rho b^2$
ρ	Fluid density
σ	Local bending slope of elastic axis $\partial h/\partial y$
τ	Local rate of change of twist along elastic axis $\partial\theta/\partial y$
ω	Circular frequency of oscillation

Symbol	Definition
SUBSCRIPTS	
i	Subscript to indicate that the parameter is associated with ith strip station of hydrofoil
n	Subscript to indicate that the parameter is perpendicular to elastic axis
SUPERSCRIPT	
$(\dot{})$	Dot over a quantity indicates differentiation with respect to time

ABSTRACT

A flutter theory based on modified Yates hydrodynamic loading was used to predict the flutter characteristics of five hydrofoil flutter models. Theoretical flutter speeds were unconservative when flutter was predicted to occur in a predominantly bending mode, and conservative when flutter was predicted to occur in a predominantly torsional mode. The theory may be useful for hydrofoils which are susceptible to flutter in a torsional mode.

ADMINISTRATIVE INFORMATION

This work was authorized and funded under the Hydrofoil Development Program of the Naval Ship Systems Command, Subproject S4606, Task 1703.

INTRODUCTION

The phenomemon of flutter involves mutual interactions among hydrodynamic, elastic, and inertial forces; therefore, a flutter potential exists for any system that is subjected to these forces. Hydrofoil flutter is conceptually identical to aeroelastic flutter of aircraft lifting-surfaces. However, hydrofoils differ significantly from airfoils in the magnitude of certain parameters relating flow characteristics to structural properties--mass ratio and reduced frequency. The magnitude of mass ratio is a determining factor in the accuracy of flutter theory.[1,2]

For typical airplane wings, mass ratio is of the order of 50; for hydrofoils and ship control surfaces, mass ratio is approximately 0.5. In the high mass-ratio region typical of airfoils, flutter theories employed in the aeronautical field in general have proven to be adequate. When these theories were extended to the low mass-ratio region typical of hydrofoils, however, flutter-speed predictions were almost invariably unconservative. Various studies have led to the belief that the classical formulations of unsteady hydrodynamic loads are not adequate.[2,3,4]

A promising approach was initiated by Yates[5] when he applied a striplike structural and hydrodynamic load theory to relatively low

---

[1]References are listed on page 43.

mass-ratio foils. Yates used a load theory which had been modified to account for three-dimensional flow effects by inserting calculated spanwise distributions of lift slope and aerodynamic center. This approach had been proven successful in predicting aerodynamic flutter.[6] When applied to a hydrofoil flutter model of mass ratio 0.99, the Southwest Research Institute (SwRI) 30-inch model,[4] the Yates theory predicted a flutter speed which was conservative by 20 percent. In view of this conservative prediction at a low mass ratio, as well as other favorable results, it was felt that the theory should be investigated further.

In his discussion of results, Yates[5] suggested that the remaining difference between theory and experiment might be due to the incomplete nature of his loading modification. The striplike loading expressions had incorporated three-dimensional effects in the circulatory loading terms; however, the noncirculatory loading terms had been left in two-dimensional form. This formulation had proved adequate in the aerodynamic mass-ratio range, where the noncirculatory terms contributed a small fraction of the total loading. However the noncirculatory terms, which include virtual mass, become relatively more important as mass ratio decreases. Therefore a three-dimensional modification to the noncirculatory portion of the loading might improve the accuracy of hydrofoil flutter predictions.

Following the Yates suggestions, the authors further modified the unsteady loading expressions used by Yates to incorporate three-dimensional effects in the noncirculatory terms. A spanwise modification factor was developed from two-dimensional virtual mass expressions and was applied to the noncirculatory terms to form a fully modified unsteady loading theory. The loading was then combined with a highly versatile, lumped-parameter structural representation to form a theory capable of predicting dynamic response and flutter characteristics of a wide range of winglike structural configurations.

To evaluate the fully modified strip theory, five different flutter models were analyzed for which experimental results were available. The mass ratios of the models ranged from 0.09 to 0.99. All models were cantilevered hydrofoils; four of the five were surface-piercing, while the fifth was fully submerged.

The analytical treatment of each model consisted of calculating the steady loading for the model, using three-dimensional lifting surface theory;[7] calculating the noncirculatory load distribution, using the expression developed by the authors; and solving the general flutter equations. To avoid convergence difficulties and numerical instability, which had presented problems in other investigations,[3,8,9] the flutter equations were solved directly rather than by the usual normal mode approach.

This report describes the complete theoretical flutter calculations, including the noncirculatory-load modification and the method of structural analysis. The five flutter models are described, and experimental and theoretical results are compared.

FLUTTER ANALYSIS

FLUTTER THEORY

Hydrofoils susceptible to flutter are generally slender, winglike structures of high aspect ratio. It is possible to represent such structures by using a straight elastic axis with structural properties lumped at discrete points along the axis. Hydrodynamic forces can be similarly lumped at stations along the axis.

In the present work, each hydrofoil model treated was divided into 10 sections. Finite-difference equations were written for the structural and fluid interactions among the foil sections according to the procedure shown in Figure 1 and described in the next paragraph. Calculations not presented in this report showed that the differences in solutions between a foil divided into 10 sections and one divided into 20 sections were negligible for the first three modes, implying that a 10-section representation gave a converged solution.

The governing equations for flutter analysis are derived by applying D'Alembert's Principle at each lumped-parameter station with proper constraint relations to account for boundary conditions. Figure 2 shows each lumped-parameter station. The flutter equations may be written in matrix form in the following manner

$$[M] \begin{Bmatrix} \ddot{h}_i \\ \ddot{\theta}_i \end{Bmatrix} + [C] \begin{Bmatrix} \dot{h}_i \\ \dot{\theta}_i \end{Bmatrix} + (1 + jg)\,[K] \begin{Bmatrix} h_i \\ \theta_i \end{Bmatrix} = \{F_i\} \qquad (1)$$

where h_i is the independent coordinate to represent the bending degree of freedom at the ith lumped-mass station, and

θ_i is the independent coordinate to represent the torsional degree of freedom at the ith lumped-mass station.

The left side of Equation (1) represents the structural characteristics of the hydrofoil. Matrix elements for the mass, damping, and stiffness matrices associated with beamlike structures such as the present hydrofoils may be derived as described in Reference 10.

The right side of Equation (1) represents the hydrodynamic force applied to the hydrofoil. The force may be expressed in the same form as the structural representation

$$-\{F_i\} = [M^*] \begin{Bmatrix} \ddot{h}_i \\ \ddot{\theta}_i \end{Bmatrix} + [C^*] \begin{Bmatrix} \dot{h}_i \\ \dot{\theta}_i \end{Bmatrix} + [K^*] \begin{Bmatrix} h_i \\ \theta_i \end{Bmatrix} \tag{2}$$

Substituting Equation (2) into Equation (1), one may arrive at the following governing matrix equation to represent the hydroelastic system

$$[\bar{M}] \begin{Bmatrix} \ddot{h}_i \\ \ddot{\theta}_i \end{Bmatrix} + [\bar{C}] \begin{Bmatrix} \dot{h}_i \\ \dot{\theta}_i \end{Bmatrix} + [\bar{K}] \begin{Bmatrix} h_i \\ \theta_i \end{Bmatrix} = \{0\} \tag{3}$$

where $[\bar{M}] = [M] + [M^*]$

$[\bar{C}] = [C] + [C^*]$

$[\bar{K}] = (1 + jg)\,[K] + [K^*]$

By assuming

$$h_i = H_i e^{st}, \text{ and } \theta_i = \Theta_i e^{st}$$

and substituting them into Equation (3), one may arrive at the following expressions

$$\left(s^2\,[\bar{M}] + s[\bar{C}] + [\bar{K}]\right) \begin{Bmatrix} H_i \\ \Theta_i \end{Bmatrix} = \{0\} \tag{4}$$

This represents a typical complex eigenvalue and eigenvector problem.

Solving Equation (4), one may obtain the complex eigenvalues of s and their corresponding eigenvectors at different speeds. Each eigenvalue corresponding to a mode of oscillation, may be written in the form

$$s = Re(s) + jIm(s)$$

or

$$s = -\zeta\omega \pm j\sqrt{1 - \zeta^2}\ \omega \quad \text{at speed V} \tag{5}$$

where Re(s) is the real part of s or the negative of the exponential decay factor = $-\delta$, and

Im(s) is the imaginary part of s or the damped natural frequency.

The variation of Re(s) of all the modes as a function of speed may be obtained from the previously described calculation. Flutter is considered to occur at the lowest speed for which Re(s) becomes zero. The corresponding flutter frequency and flutter mode are given by Im(s) and its eigenvector, respectively.

The dynamic characteristics of the structure in vacuum and in water at zero speed may be obtained from Equation (3) by omitting certain terms. First, by neglecting all the unsteady hydrodynamic forces and all damping elements, Equation (3) becomes

$$[M] \begin{Bmatrix} \ddot{h}_i \\ \ddot{\theta}_i \end{Bmatrix} + [K] \begin{Bmatrix} h_i \\ \theta_i \end{Bmatrix} = \{0\} \tag{6}$$

Solving Equation (6), one may obtain the natural frequencies of the structure and its associated mode shapes in vacuum. Second, by including the virtual mass matrix [M*] in Equation (6), one obtains

$$[\bar{M}] \begin{Bmatrix} \ddot{h}_i \\ \ddot{\theta}_i \end{Bmatrix} + [K] \begin{Bmatrix} h_i \\ \theta_i \end{Bmatrix} = \{0\} \tag{7}$$

The solution of Equation (7) gives the natural frequencies and associated mode shapes of the structure in water at zero speed.

A digital computer program[11] has been used to solve Equations (4), (6), and (7) on the CDC 6700 computer at the Center.

FLUTTER MODELS

The hydrofoils selected for this study were the SwRI 30-inch flutter model,[4] Grumman Models 1, 2, and 3,[8] and Grumman Model A.[9] All the models had very low mass ratio, ranging from 0.09 to 0.99. All except the SwRI model had been tested as partly submerged foils perpendicular to the water surface. The SwRI model had been tested fully submerged with a reflection plate at its root. The detailed characteristics of each model are summarized in the Appendix.

HYDRODYNAMIC LOADING

As shown in Equation (2), expressions for hydrodynamic lift and moment are required as functions of the foil displacements h and θ and the corresponding velocities and accelerations. In the original Yates treatment,[6] the circulatory part of the classical Theodorsen two-dimensional load theory[12] was modified to include calculated or measured spanwise lift-slope and aerodynamic-center distributions. In accordance with the Yates suggestion,[5] the authors made an additional modification to the loading used by Yates. The additional modification consisted of a reduction in the magnitude of the noncirculatory loading along the span of loaded surfaces in order to account for three-dimensional flow effects. A reduction factor resembling the distribution of virtual mass on a flat plate was chosen. In the following sections, the location of the modification in the Yates loading expressions is given, and the method of calculating the modification is described. In addition, the method is described for calculating the lift-slope and aerodynamic-center distributions required for the circulatory modification, and the calculated distributions are given.

MODIFIED YATES LOADING

The unsteady hydrodynamic expressions which Yates applied to each strip along the span of the foil were similar in form to the expressions presented in Reference 13 for the lift and pitching moment on a section of a wing oscillating harmonically in two-dimensional incompressible flow at a nonzero sweep angle. Yates reformulated[6] the expressions to permit the use of arbitrary values of steady lift-curve slope and section aerodynamic center, instead of the values 2π and quarter chord, respectively,

the results of two-dimensional thin airfoil theory. The required spanwise distributions of section lift-curve slope and section aerodynamic center for a particular planform may be obtained by any reliabile theoretical or experimental method. For the present analysis they were obtained from the kernel-function type of lifting-surface theory presented in Reference 7.

Modification of noncirculatory loading was made with a multiplicative factor p_i, inserted in the Yates unsteady loading expressions as follows

$$-P_i = p_i \pi \rho b_i^2 \left[\ddot{h}_i - V_n \dot{\theta}_i + V_n \dot{\sigma}_i \tan \Lambda_{ea} + b_i a_i \left(\ddot{\theta}_i + V_n \dot{\tau}_i \tan \Lambda_{ea} \right) \right] - C_{\ell_{\alpha,i}} \rho V_n b_i \, C(k) \, w_i$$

$$-M_i = p_i \pi \rho b_i^4 \left(1/8 + a_i^2 \right) \left(\ddot{\theta}_i + V_n \dot{\tau}_i \tan \Lambda_{ea} \right) + p_i \pi \rho b_i^2 V_n \left(\dot{h}_i + V_n \sigma_i \tan \Lambda_{ea} \right)$$

$$+ p_i \pi \rho b_i^3 a_i \left(\ddot{h}_i + V_n \dot{\sigma}_i \tan \Lambda_{ea} \right) - p_i \pi \rho b_i^2 V_n^2 \left(\theta_i - a_i b_i \tau_i \tan \Lambda_{ea} \right)$$

$$+ 2\pi \rho V_n b_i^2 \left[\frac{1}{2} p_i - \left(a_i - a_{c,i} \right) \frac{C(k) \cdot C_{\ell_{\alpha,i}}}{2\pi} \right] w_i \qquad (8)$$

where

$$w_i = -\dot{h}_i + V_n \theta_i - V_n \sigma_i \tan \Lambda_{ea} + b_i \left(\frac{C_{\ell_{\alpha,i}}}{2\pi} + a_{c,i} - a_i \right) \left(\dot{\theta}_i + V_n \tau_i \tan \Lambda_{ea} \right)$$

These expressions were formulated on the basis of hydrofoil sections oriented normal to the hydrofoil elastic axis, although an analogous procedure would apply for streamwise sections. If the modification factor p_i were set equal to 1 in the previous expressions, the loading would be that used by Yates. Three-dimensional flow effects reduce sectional values of p_i to less than 1.

NONCIRCULATORY MODIFICATION FACTOR

In attempting to develop an expression for the spanwise modification factor p_i, the literature was consulted for solutions to the problem of a nonlifting three-dimensional body, oscillating in a fluid medium with or

without a free surface. References 14 and 15 gave some general approaches in this area; however, no useful analytical expressions have been derived. Therefore, in view of the presence of virtual mass and moment in the non-circulatory loading, the modification factor in the absence of a free surface was inferred from the distribution of virtual mass on a flat plate oscillating normal to its own plane. The factor consisted of the three-dimensional virtual mass of the plate, expressed as a fraction of the two-dimensional virtual mass, outboard of the spanwise position being considered. This quantity may be expressed as a spanwise function of the local aspect-ratio A_i^* of the ith section in the form

$$p_i = \frac{A_i^*}{\sqrt{1 + (A_i^*)^2}} \tag{9}$$

For the limiting case of infinite aspect ratio, corresponding to a two-dimensional hydrofoil, p_i is equal to 1.

A different modification factor is required for high-frequency motion when a free surface is present. By referring to a solution of the two-dimensional problem of a cylinder swaying in a fluid medium while piercing the free surface,[16] it was found that the pressure loading on a thin plate was strongly dependent on the nondimensional frequency $\ell\omega^2/g$. As shown in Figure 3, large values of $\ell\omega^2/g$ result in pressure distributions which decrease to zero at the free surface, while the pressure approaches the free surface near its maximum value for small values of $\ell\omega^2/g$. Therefore for values of $\ell\omega^2/g$ of 10 or greater, a free surface effect must be included in the modification factor. The free surface may be considered a reflecting plane for values of $\ell\omega^2/g$ of 1 or less. For hydrofoils in general, $\ell\omega^2/g$ is very large; hence, the distribution of p_i should be similar to the curve with $\ell\omega^2/g = \infty$. To simulate this distribution in the present report, Equation (9) was used to calculate the values of p_i by considering the midspan of the hydrofoil to be a reflecting plane.

Total virtual mass values given by the low-frequency version of the formula agreed well with measured values reported in Reference 8, while the high-frequency version showed only fair agreement. This comparison is shown in Figure 4. No frequency data were given in Reference 8 to

enable determination of the experimental nondimensional frequency. Average values of the function p_i over each hydrofoil section were used in the flutter computation.

Figure 5 shows two distributions of p_i. The curve shown for the SwRI 30-inch model corresponds to a reflecting plane at the root of the model. The curve shown for Grumman Model 1 has incorporated a free-surface condition by considering the midspan of the foil to be a reflecting plane. The value of $\ell\omega^2/g$ for Grumman Model 1 was 32 at flutter, and therefore the free surface condition was appropriate. When $\ell\omega^2/g$ is not known for a surface-piercing model at flutter, a value may be assumed, using perhaps the first torsional frequency. If the calculated flutter frequency were significantly different, the free-surface boundary condition could be changed and the flutter characteristics recalculated.

STEADY LIFT AND AERODYNAMIC CENTER DISTRIBUTIONS

In accordance with the procedure used by Yates,[6] the spanwise distributions of lift and aerodynamic center of the hydrofoils were calculated by lifting-surface theory. Although unsteady lift and aerodynamic center can be calculated by lifting-surface theory, only steady loading distributions can be used in the Yates unsteady loading formulation. Therefore the results obtained are a quasi-steady approximation to the exact unsteady loading characteristics.

A lifting-surface theory developed and programmed for the IBM 7090 computer by Widnall[7] has been used in the present work. This theory can treat three-dimensional planar and nonplanar foil configurations that are assumed to be of zero thickness and at small angles of attack. Surface-piercing and finite-depth configurations at infinite Froude number can be treated as well as infinite-depth configurations.

The Widnall theory has not been fully evaluated for agreement with either other calculations or experiments or for numerical convergence. However, available calculations agree with other lifting-surface theories and are accurate at low-aspect ratios (less than 3) and inaccurate at high-aspect ratios (more than 3) when compared to experiments. Some numerical convergence difficulties also occur at high aspect ratios. In view of the agreement with other theories and the extreme versatility of the Widnall

theory, it has been used for the present steady loading calculations. It is recommended that the sensitivity of the flutter calculation to variations in lift slope and center of pressure be determined, particularly at high aspect ratio.

Steady loading was required for each flutter model in the form of lift slope and aerodynamic center as functions of spanwise position. These quantities were calculated by assuming a uniform angle of attack along the entire span of the foil. While it would be possible to simulate a calculated- or measured-mode shape by choosing a varying angle of attack, the lift slope and aerodynamic center for a first torsion mode were similar to those for the uniform angle over most of the foil. Effects on loading due to varying deflection were therefore regarded as second order effects suitable for future investigation.

Figure 6 shows the load characteristics calculated for the five flutter models. All models except the SwRI 30-inch model were only partially submerged, so their load distributions began at the spanwise position corresponding to the waterline. The boundary condition at the free surface was determined in the same manner as for the noncirculatory load-modification factor described previously. For values of the nondimensional frequency $\ell\omega^2/g$ much greater than 1, a high-frequency condition, the antisymmetrical boundary condition was invoked, resulting in lift slopes that dropped to zero at the free surface. For $\ell\omega^2/g \ll 1$, or low frequencies, the free surface was treated as a reflecting plane which supported symmetrical loading. Ultimately, the frequency used for this determination would be the calculated flutter frequency. As described previously, a preliminary estimate could be made using the first torsional frequency, subject to the outcome of the flutter calculation. It was determined that Grumman Models 1, 2, and 3 had high-frequency load characteristics, while Grumman Model A had low-frequency characteristics. The SwRI 30-inch model was attached to a root-reflecting plate during testing.

STRUCTURAL VIBRATION CHARACTERISTICS

Natural frequencies and associated mode shapes of the five models selected in this study were computed. The mode shapes were expressed in terms of nodal lines. Both analytical results and experimental data are

presented in the following sections. The analytical calculations show very good agreement with experimental results. Hence, it is felt that the mathematical model used for the flutter analysis adquately represents the structural characteristics of the models.

SwRI 30-INCH FLUTTER MODEL

Table 1 gives the calculated and measured natural frequencies for the SwRI 30-inch flutter model in vacuum, and Table 2 gives the calculated and measured natural frequencies in water. Table 3 shows the calculated and measured first coupled bending mode shape in vacuum and first coupled torsional mode shape in vacuum. Figures 7 and 8 show the calculated nodal lines in vacuum and in water, respectively. No experimental results on measured nodal lines are available.

GRUMMAN MODEL 1

Table 4 gives the calculated and measured natural frequencies for Grumman Model 1 in vacuum. Table 5 gives the analytical natural frequencies in water; no test data are available. For this particular model, the elastic axis coincides with the center of gravity, and is also at the midchord of the hydrofoil. Therefore, at zero speed, it is a decoupled bending and torsion system, either in vacuum or in water. Figures 9 and 10 show the calculated nodal lines in vacuum and in water, respectively. Only the nodal lines in air have been measured,[8] and they are included in Figure 9.

GRUMMAN MODEL 2

Table 6 gives calculated and measured natural frequencies for Grumman Model 2 in vacuum. Table 7 gives the analytical natural frequencies in water; no test data are available. Figures 11 and 12 give the analytical nodal lines in vacuum and in water, respectively. Only the nodal lines in air have been measured,[8] and they are included in Figure 11. It is interesting to note that the order of the fifth and sixth modes in vacuum was reversed when the model was in water.

GRUMMAN MODEL 3

Tables 8 and 9 give the analytical natural frequencies for Grumman Model 3 in vacuum and in water, respectively. The analytical nodal lines in vacuum and in water are also shown in Figures 13 and 14, respectively. No experimental data are available for either natural frequencies or nodal lines.

GRUMMAN MODEL A

Calculated and measured natural frequencies for Grumman Model A in vacuum are given in Table 10. Analytical natural frequencies in water are given in Table 11; no test data are available. The calculated nodal lines in vacuum and in water, along with the measured nodal lines in air, are shown in Figures 15 and 16, respectively.

FLUTTER RESULTS

SwRI 30-INCH FLUTTER MODEL

The SwRI 30-inch flutter model underwent structural failure due to flutter at a speed of 48.1 knots and a frequency of 17.5 Hz, as described in Reference 4. Measured values of exponential decay factor and oscillation frequency for the unstable mode are shown in Figures 17 and 18, respectively.

Many flutter calculations have been published for this model. Figures 17 and 18 show the results of four published calculations as Theories 1 through 4. These calculations contained no empirical corrections. All four of the theories gave drastically unconservative predictions of flutter speed, the closest agreement with experiment being obtained from the generalized lifting surface theory of Reference 3 at 67.5 knots.

In contrast to the unconservative predictions of the previously described theories, two calculations based on Yates hydrodynamic loading gave conservative results. The calculation using unmodified Yates loading, identified as Theory 5 in Figures 17 and 18, predicted an overconservative flutter speed of 30 knots. It is felt that the difference between the present result, which was conservative by 38 percent, and the original Yates result,[5] which was conservative by 20 percent, was due to numerical approximations accentuated by the nearly horizontal orientation of the

damping curve. An improved result, shown as Theory 6, was obtained using modified Yates loading. The modified Yates theory gave a flutter speed of 40.5 knots, which was 16 percent conservative, and, in contrast to all of the other theories, showed good agreement with measured damping values. Both of these calculations assumed a value of 0.02 for the structural damping parameter g. All of the predicted frequencies followed the measured frequencies fairly well over the observed range, and corresponded to the second mode of response.

GRUMMAN MODELS 1, 2, AND 3

A description of the flutter testing of Grumman Models 1, 2, and 3 is given in Reference 8. The models were accelerated until flutter occurred; the speed at which flutter stopped during deceleration was taken as the flutter speed. Figures 19 through 21 show the observed flutter characteristics.

Three published flutter speed predictions for Model 1, shown as Theories 1, 2, and 3 in Figure 19, were grossly unconservative when compared with the experimental flutter speed of 66 knots. Both of the flutter calculations based on Yates hydrodynamic loading, shown as Theories 4 and 5 in Figure 19, were similarly unconservative. Using unmodified Yates loading, a flutter speed of 118 knots was obtained, which was 79 percent above the experimental value. A more unconservative result was obtained with modified Yates loading which gave a flutter speed of 148 knots, 124 percent above experiment. The predicted and observed frequencies agreed fairly well as functions of speed, including a "dead beat" point at 36 knots, obtained from the test log.* Flutter was predicted to occur in the first mode of response.

The model response characteristics calculated for Model 2 using both Yates and modified Yates loading, are shown in Figure 20. Flutter occurred experimentally at 81 knots. The Yates analysis predicted a flutter speed of 87 knots, which was unconservative by 7 percent. After modification

*Private communication with Mr. Charles E. Squires, Jr., Grumman Aerospace Corporation.

to the loading, a flutter speed of 104 knots was calculated, 28 percent above experiment. Frequency predictions for Model 2 followed the observed frequencies fairly well as a function of speed. The frequencies between 84 and 100 knots were obtained from the experimental log book.* Flutter was again predicted to occur in the first mode of response.

There was little difference in the response characteristics calculated for Model 3 using the two versions of Yates loading (see Figure 21). The calculations gave a flutter speed of 61 knots for the Yates analysis and a slightly higher flutter speed of 63 knots for the modified Yates analysis. These predictions were approximately 30 percent above the experimental value of 48 knots. The predicted frequency curves agree fairly well with the frequency observed during flutter.

GRUMMAN MODEL A

Figure 22 shows flutter test results for Grumman Model A along with two previously published flutter predictions and the two present Yates analyses. The flutter results were taken from Reference 9 and corresponded to a sweep angle of 5 degrees.

Theory 1 in Figure 22, based on two-dimensional Theodorsen loading, agreed exactly with the experimental flutter speed of 32.5 knots. Theory 2, a generalized lifting surface theory, gave an unconservative flutter speed of 47.2 knots, 45 percent above experiment. The Yates analysis shown as Theory 3, was 14 percent unconservative in its prediction of 37 knots. A low-frequency free surface condition was assumed for this calculation.

The modified Yates analysis was made with two free surface conditions for comparison. As previously described, a low frequency surface-piercing foil should be treated as though the free surface were a reflecting plane. Because the nondimensional frequency $\ell\omega^2/g$ was 0.35 for Model A at flutter, a low-frequency condition was assumed in calculating the theoretical Curve 4a in Figure 22. An unconservative flutter speed of 38 knots was obtained, 17 percent above the experimental value. When the high-frequency surface condition was used in calculating Theory 4b, the less

*Refer to footnote on page 13.

accurate flutter speed of 42 knots obtained was 29 percent unconservative. It is concluded that the free surface condition to be used in calculating the noncirculatory loading modification should be determined by the nondimensional frequency of the hydrofoil at flutter.

All theoretical approaches except Theory 2 gave accurate frequency predictions at the speed at which flutter occurred experimentally. As obtained for the other surface-piercing struts, the analyses based on different forms of Yates loading predicted that flutter instability would occur in the first mode of response.

DISCUSSION

The two Yates flutter analyses did not show general agreement with experimental results. Conservative predictions were obtained for the SwRI 30-inch model, a fully-wetted strut with a mass ratio of 0.99. Unconservative predictions were obtained for Grumman Models 1, 2, 3, and A; these were surface-piercing struts with mass ratios between 0.09 and 0.28. The modified Yates analysis always gave a higher flutter speed than the unmodified analysis. Therefore the noncirculatory load modification improved the results for the SwRI model and worsened the predictions for the surface-piercing struts.

An interesting pattern was observed in the modes of response of the flutter models. The conservative and unconservative flutter speed predictions differed in the predicted flutter mode. When conservative results were obtained, flutter was predicted to occur in the second mode of response, with deflections primarily resembling the fundamental torsion mode of a cantilever beam. Unconservative results were always associated with the first mode of response, resembling the fundamental bending mode of a cantilever beam. The predicted frequencies agreed well with observed frequencies, and therefore it is felt that the predicted flutter modes were the ones that actually occurred. The tendency of the two Yates analyses to be conservative or unconservative in flutter predictions appears to be associated with the mode of response at flutter.

Several hydrodynamic factors differed among the models, but they were not felt to be responsible for the differences in the flutter modes. These hydrodynamic factors were mass ratio, submergence, sweep angle, and

profile. Rather than these factors, it is felt that differences in structural properties of the models caused the variation in flutter modes. The structural differences may be observed in the two groupings of structural modes which appear in Figures 7 through 16. The SwRI 30-inch model displayed a first bending mode followed by a first torsion mode, while the Grumman models displayed a first bending mode followed by a second bending mode. The latter models displayed a first torsion mode in the third position. These two mode sequences occurred both in vacuum and in water. The mode sequence variation was caused by a difference in the relative stiffness of bending and torsion, and in the mass distribution, of the two types of models. The SwRI 30-inch model had a relatively greater tendency to oscillate in torsion than the other models.

On the basis of the above correlation, it is concluded that the Yates analysis and the modified Yates analysis may be useful in obtaining conservative hydrofoil flutter speed predictions for flutter which occurs in a torsional mode. Further correlation with data is required to confirm this conclusion. It does not appear that these analyses are useful for predominantly bending flutter. Additional investigation of the hydrodynamics is required in order to obtain improved results for bending flutter. In particular, this investigation should include a determination of the sensitivity of the flutter calculation to variations in spanwise input parameters. Important parameters should then be checked with available data. The entire hydrodynamic loading formulation should be compared with data given in References 18 and 19.

None of the other theories presented except the two-dimensional Theodorsen gave conservative predictions for any of the hydrofoils. The Theodorsen theory gave exact agreement for a bending flutter occurrence but an unconservative prediction for the torsional case. Therefore none of the other theories appear to be useful in treating hydrofoil flutter of either the bending or the torsional type.

CONCLUSIONS

1. The Yates analysis and the modified Yates analysis may be useful in obtaining conservative hydrofoil flutter speed predictions for flutter which occurs in a torsional mode. It does not appear that these analyses are useful for predominantly bending flutter.

2. Both Yates analyses are capable of giving fairly accurate predictions of frequency as a function of speed.

3. The other theories used for comparison with the Yates theories do not appear to be useful in treating hydrofoil flutter of either the bending or the torsional types.

4. Structural characteristics of the flutter models were adequately represented by the lumped-parameter mathematical model.

5. The free-surface condition to be applied in calculating the noncirculatory loading modification for a surface-piercing hydrofoil should be determined according to the nondimensional frequency of the hydrofoil at flutter.

RECOMMENDATIONS

1. Further correlation with data is recommended to establish the validity of the Yates theories in treating predominantly torsional flutter, as compared to predominantly bending flutter, of hydrofoils.

2. Additional investigation of the hydrodynamics is required in order to obtain improved results for bending flutter. In particular, this investigation should include a determination of the sensitivity of the flutter calculation to variation in spanwise input parameters. Important parameters should then be checked with available data. The entire hydrodynamic loading formulation should be compared with the data given in References 18 and 19.

ACKNOWLEDGMENTS

The authors are grateful to the following people for their contributions to the present work: Dr. C. M. Lee who calculated the pressure distributions on a swaying plate; Mr. J. R. Caspar who assisted in obtaining computer results; and Mr. S. E. Lee and Mr. D. S. Cieslowski who provided constructive criticism and overall guidance.

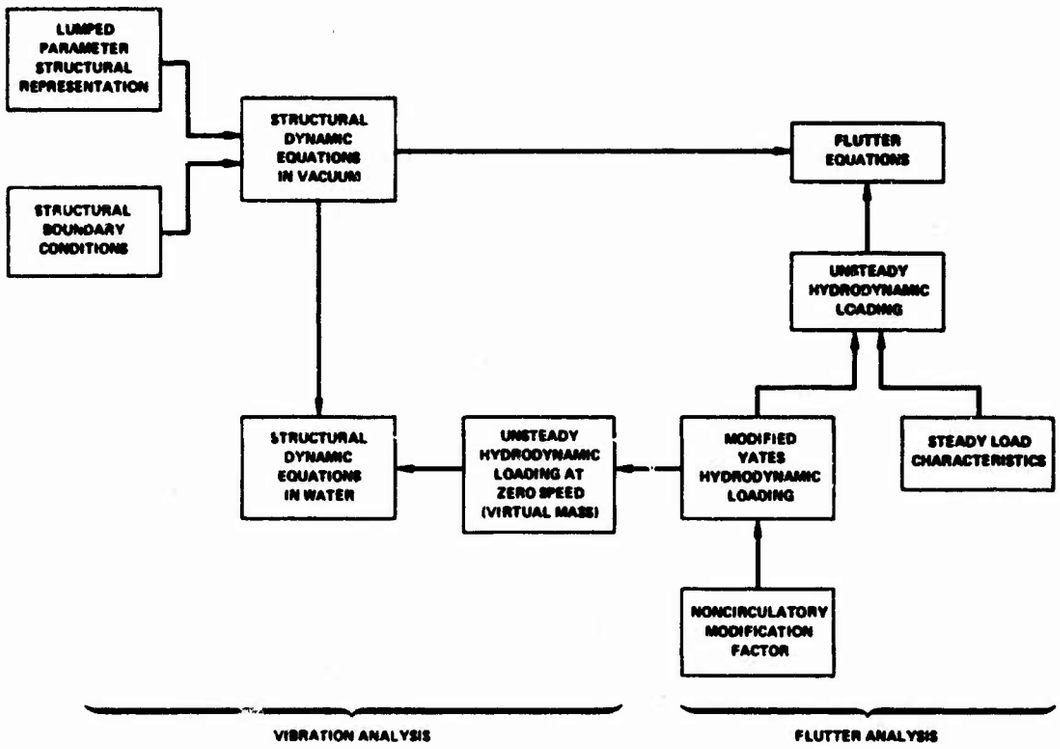

Figure 1 - Flow Diagram of Hydrofoil Hydroelastic Analysis

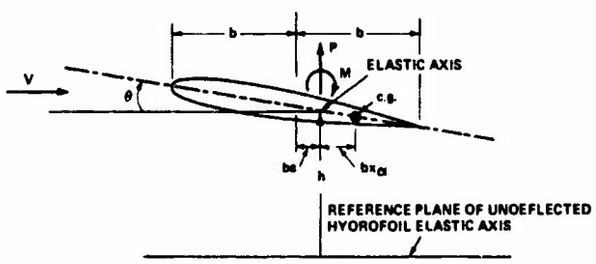

Figure 2 - Representative Hydrofoil Section

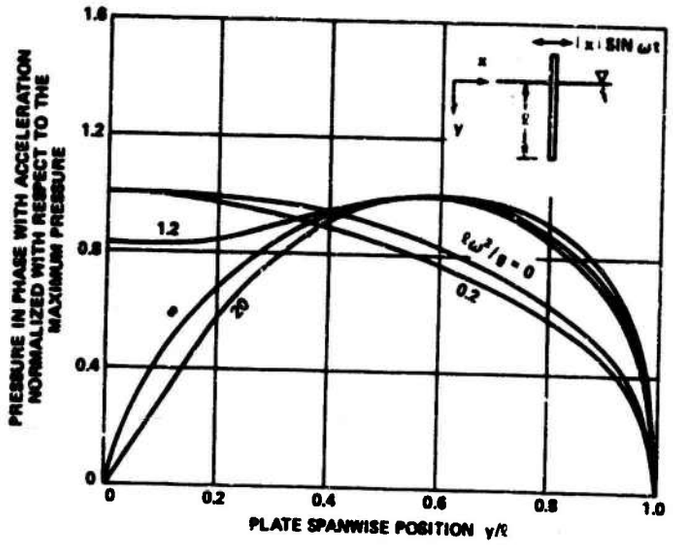

Figure 3 - Pressure in Phase with Acceleration as a Function of Spanwise Position on a Swaying Plate

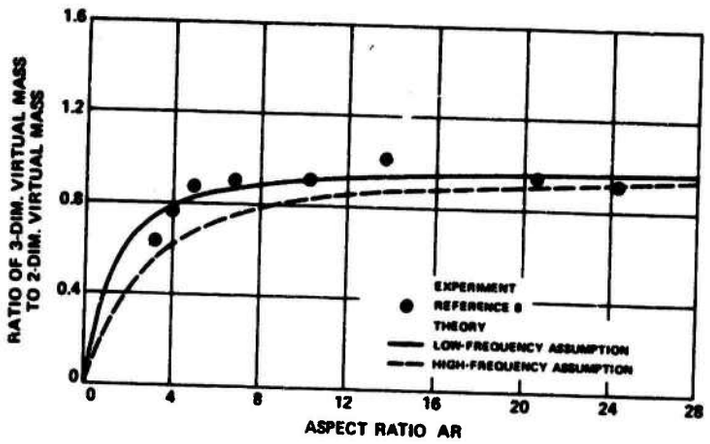

Figure 4 - Virtual Mass as a Function of Aspect Ratio for Cantilever Hydrofoils with Free Surface

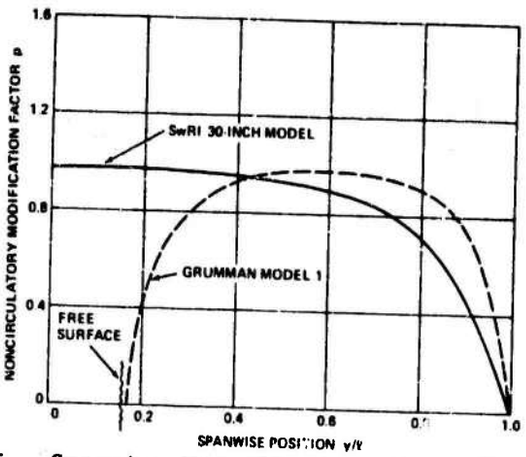

Figure 5 - Spanwise Distribution of Noncirculatory Modification Factor

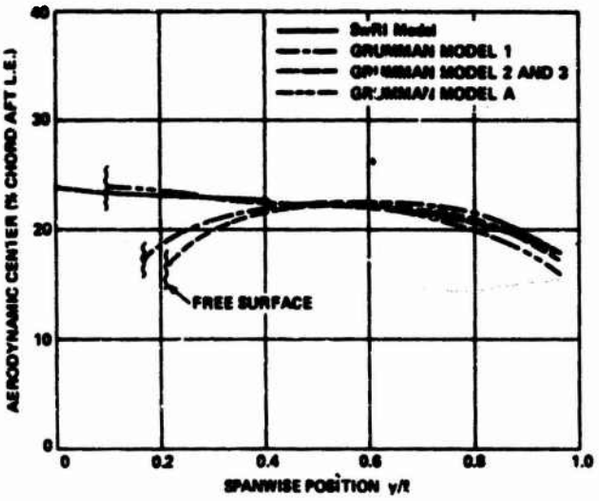

Figure 6a - Spanwise Distribution of Aerodynamic Center

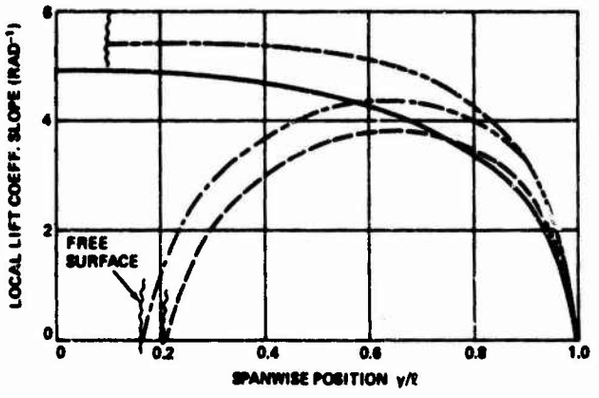

Figure 6b - Spanwise Distribution of Lift Coefficient Slope

Figure 6 - Steady Hydrodynamic Loading Characteristics

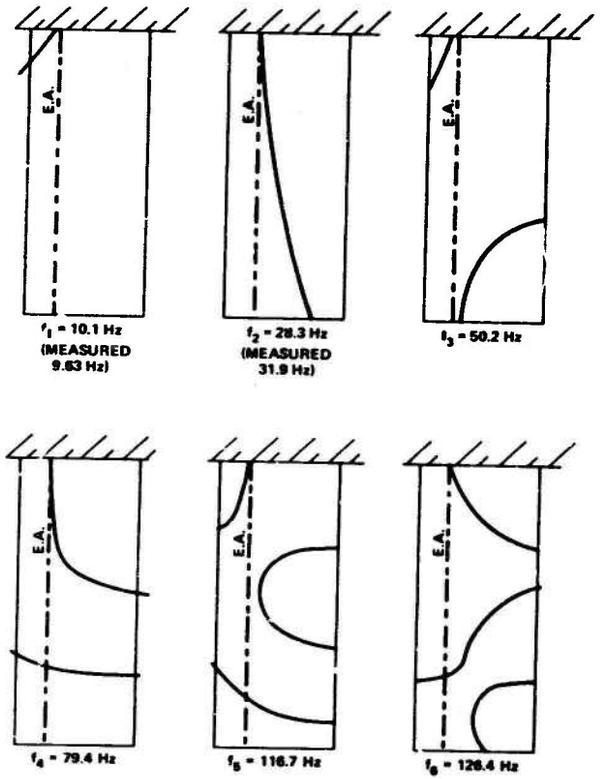

Figure 7 - Analytical Nodal Lines in Vacuum for the SwRI 30-Inch Flutter Model

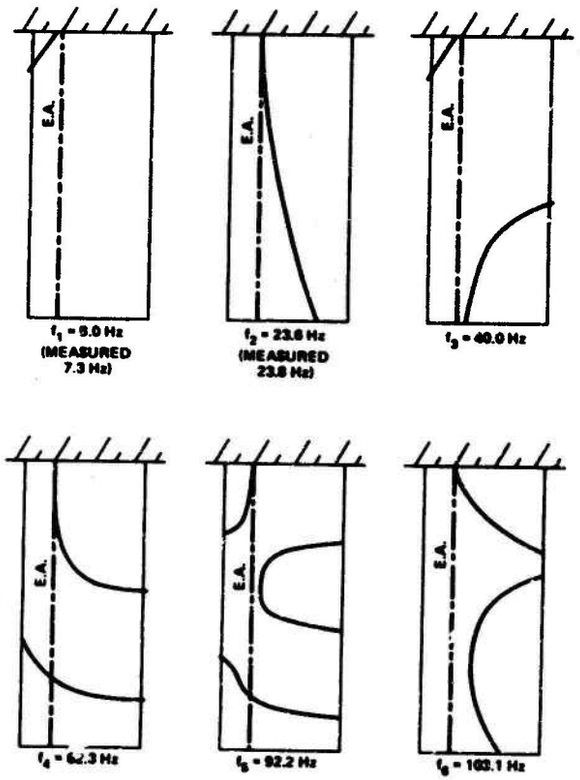

Figure 8 - Analytical Nodal Lines in Water for the SwRI 30-Inch Flutter Model

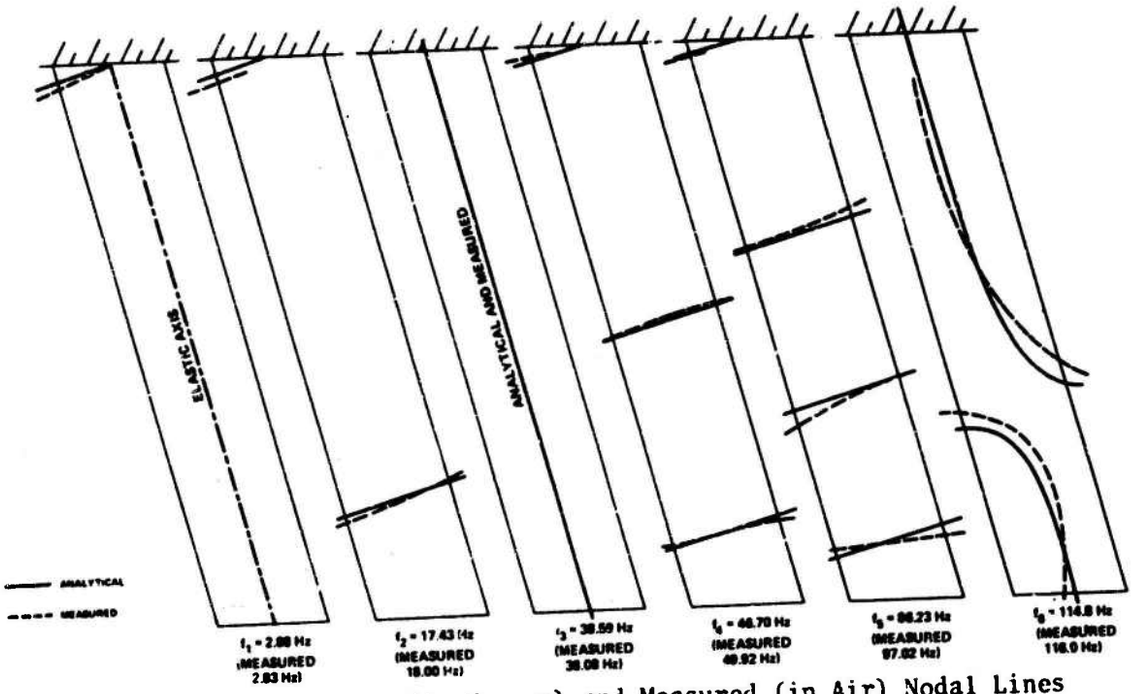

Figure 9 - Analytical (in Vacuum) and Measured (in Air) Nodal Lines for Grumman Model 1

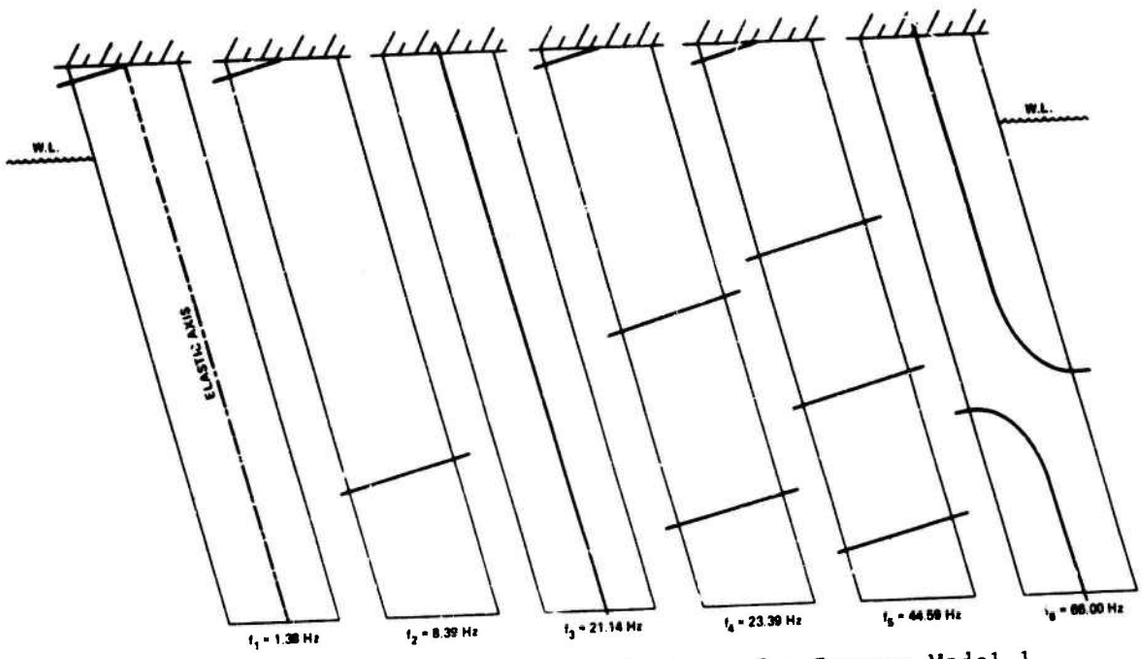

Figure 10 - Analytical Nodal Lines in Water for Grumman Model 1

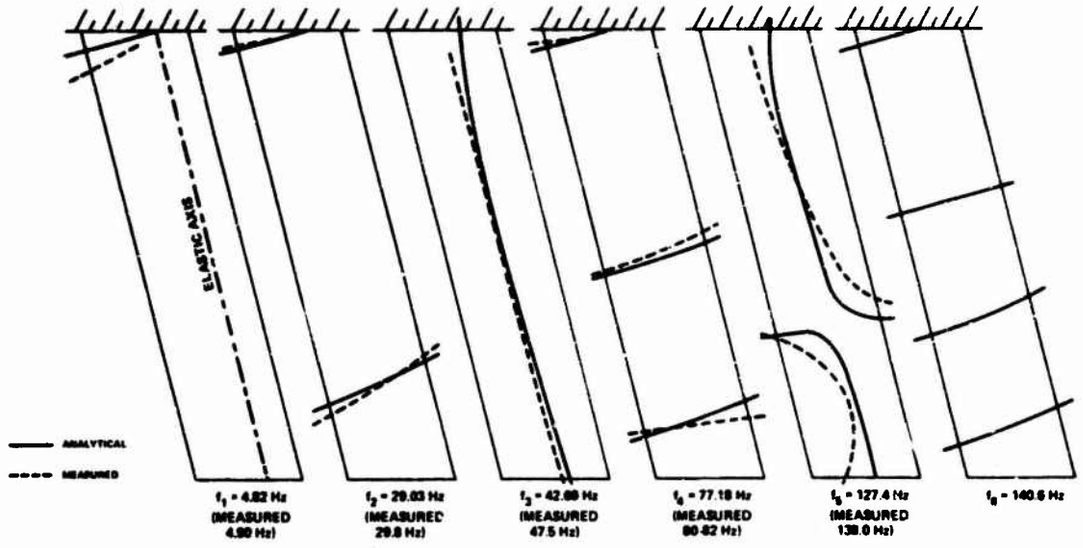

Figure 11 - Analytical (in Vacuum) and Measured (in Air) Nodal Lines for Grumman Model 2

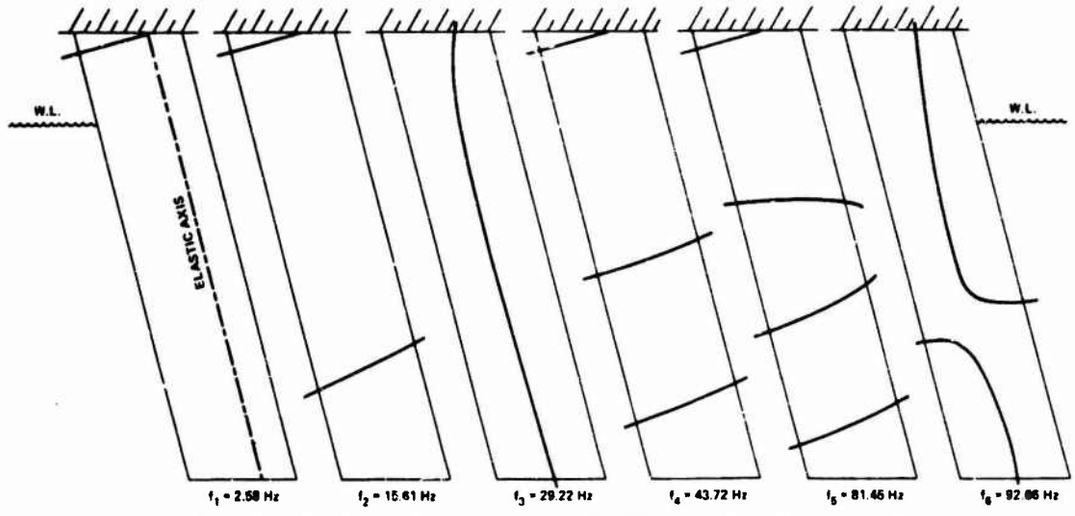

Figure 12 - Analytical Nodal Lines in Water for Grumman Model 2

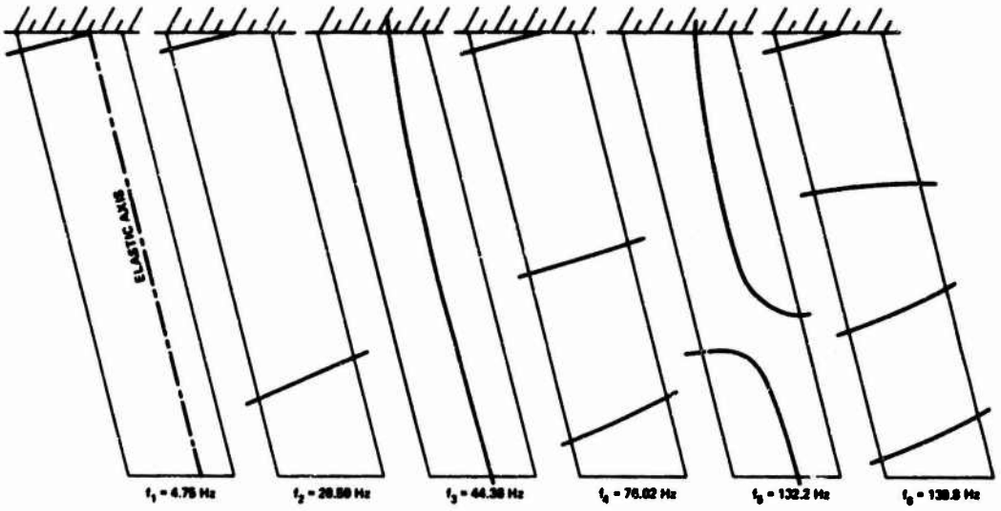

Figure 13 - Analytical Nodal Lines in Vacuum for Grumman Model 3

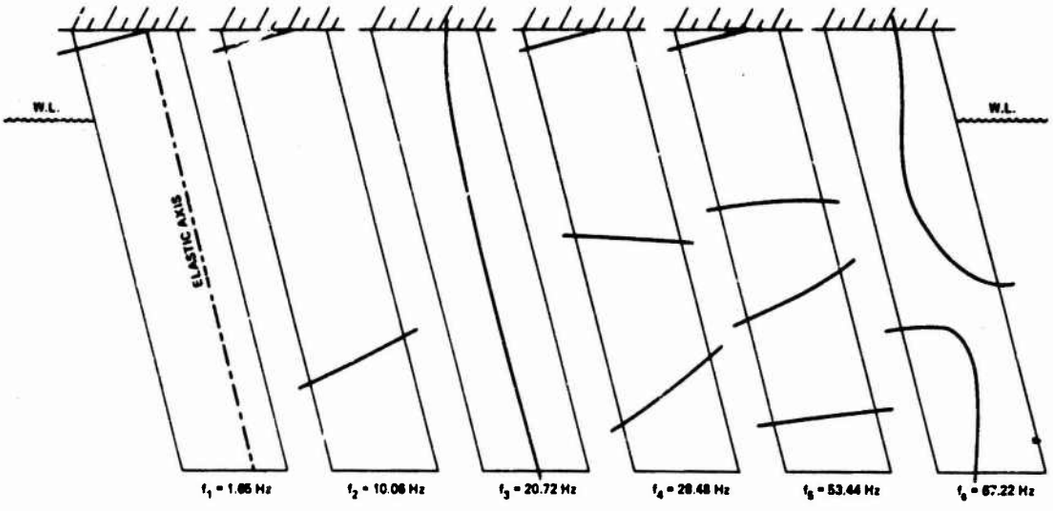

Figure 14 - Analytical Nodal Lines in Water for Grumman Model 3

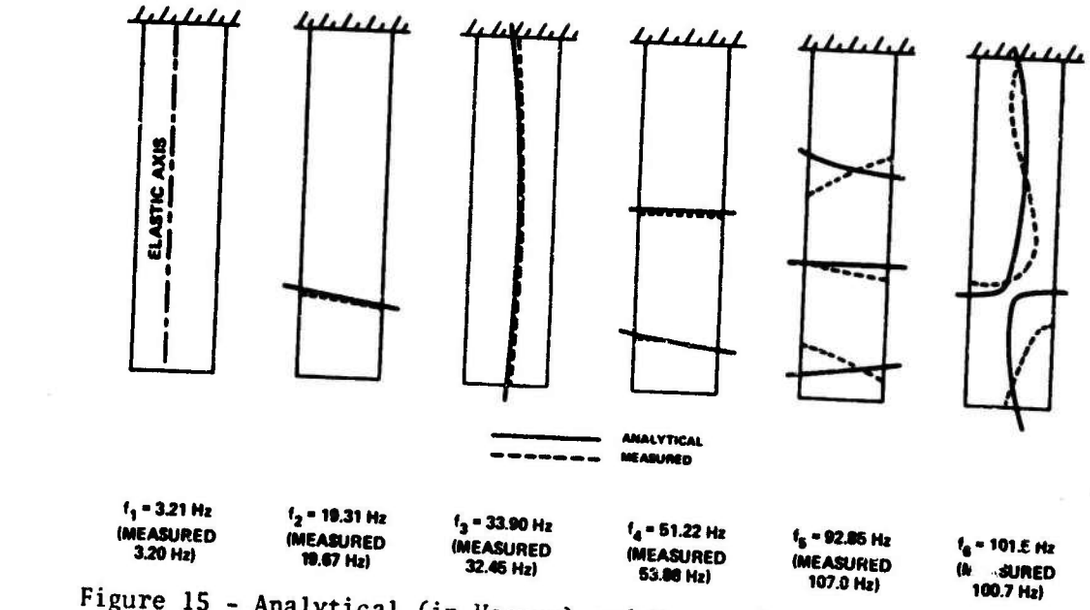

Figure 15 - Analytical (in Vacuum) and Measured (in Air) Nodal Lines for Grumman Model A

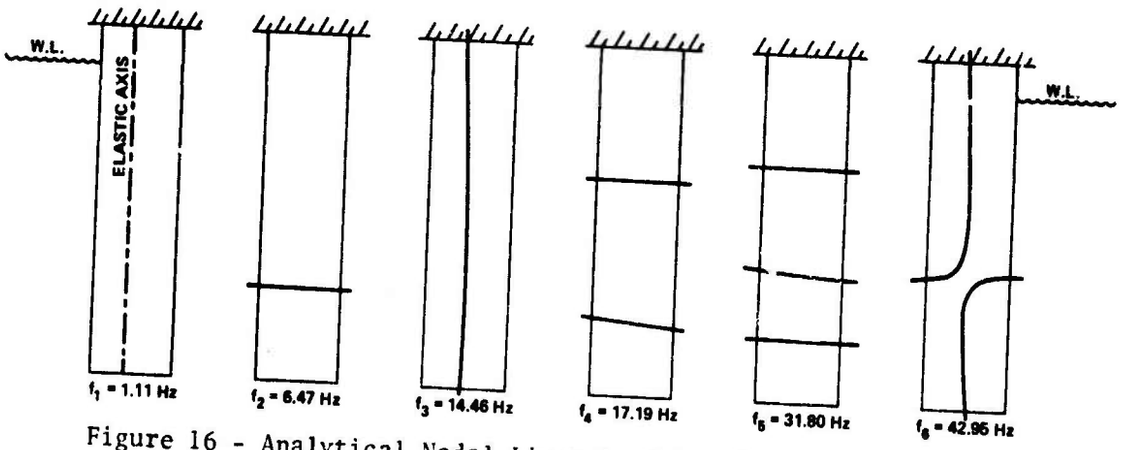

Figure 16 - Analytical Nodal Lines in Water for Grumman Model A

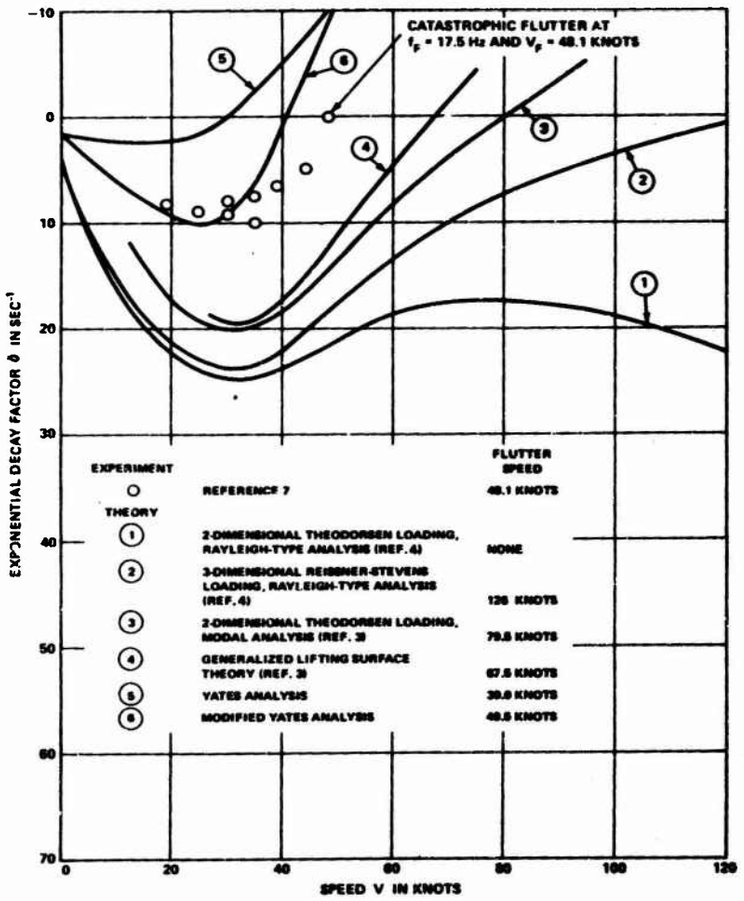

Figure 17 - Exponential Decay Factor δ as a Function of Speed for the SwRI 30-Inch Flutter Model

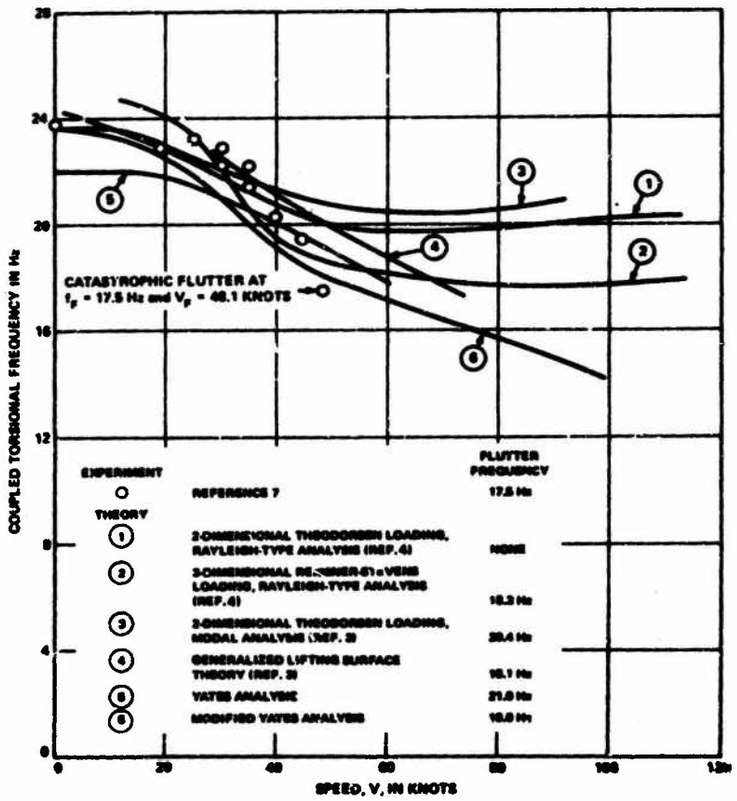

Figure 18 - Coupled Torsional Frequency as a Function of Speed for the SwRI 30-Inch Flutter Model

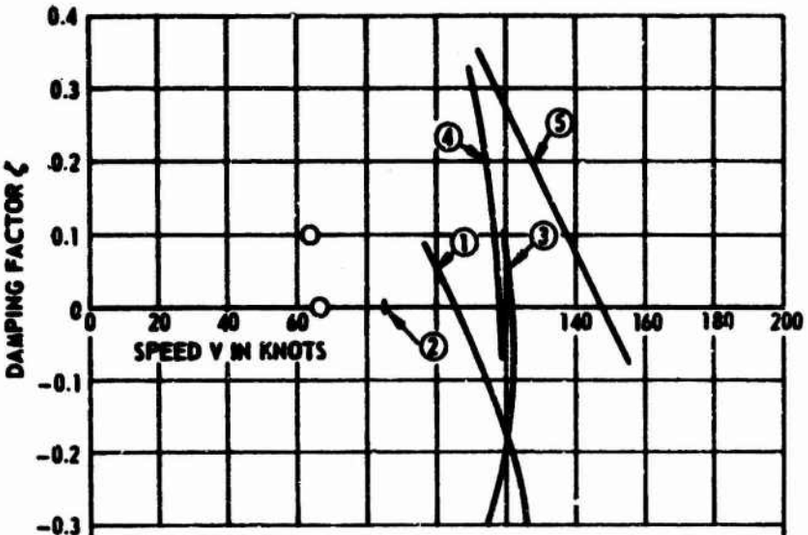

Figure 19a - Damping Factor ζ

EXPERIMENT		FLUTTER SPEED	FLUTTER FREQUENCY
○	REFERENCE 8	66.8 KNOTS	2.5 HZ
THEORY			
①	TWO-DIMENSIONAL THEODORSEN LOADING, MODAL ANALYSIS (REF. 3)	105.0 KNOTS	6.3 HZ
②	TWO-DIMENSIONAL STRIP THEORY, MODAL ANALYSIS (REF. 8)	85.0 KNOTS	3.6 HZ
③	GENERALIZED LIFTING SURFACE THEORY (REF. 3)	122.0 KNOTS	8.8 HZ
④	YATES ANALYSIS	118.8 KNOTS	5.8 HZ
⑤	MODIFIED YATES ANALYSIS	140.0 KNOTS	10.5 HZ

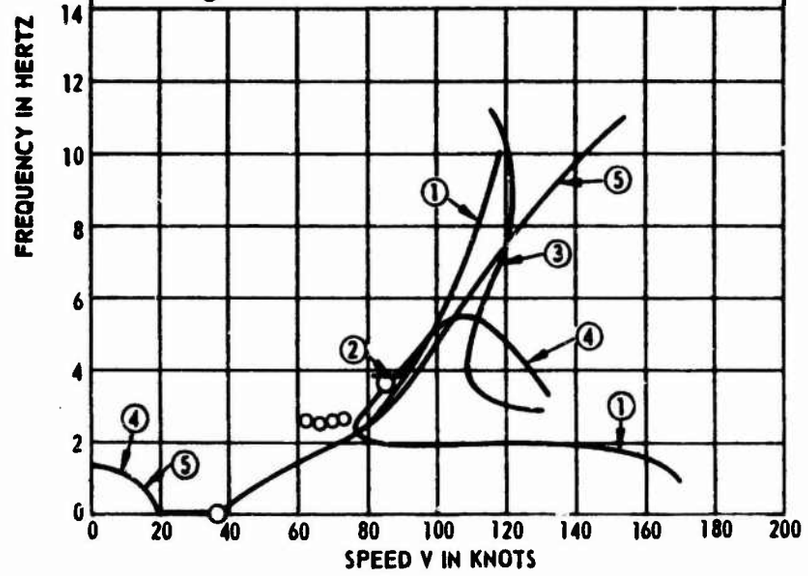

Figure 19b - Frequency

Figure 19 - Critical Flutter Modes as Functions of Speed for Grumman Model 1

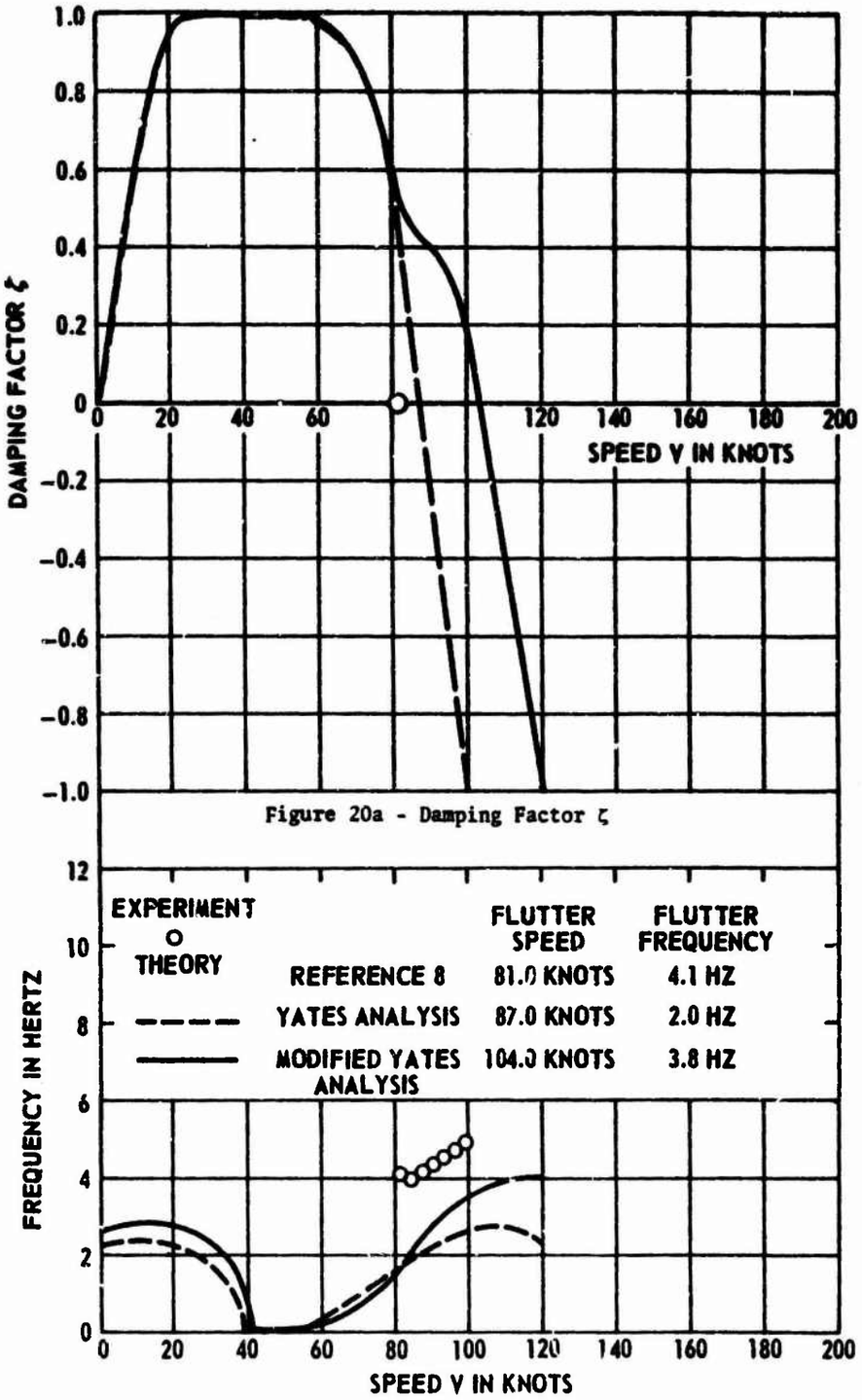

Figure 20a - Damping Factor ζ

Figure 20b - Frequency

Figure 20 - Critical Flutter Modes as Functions of Speed for Grumman Model 2

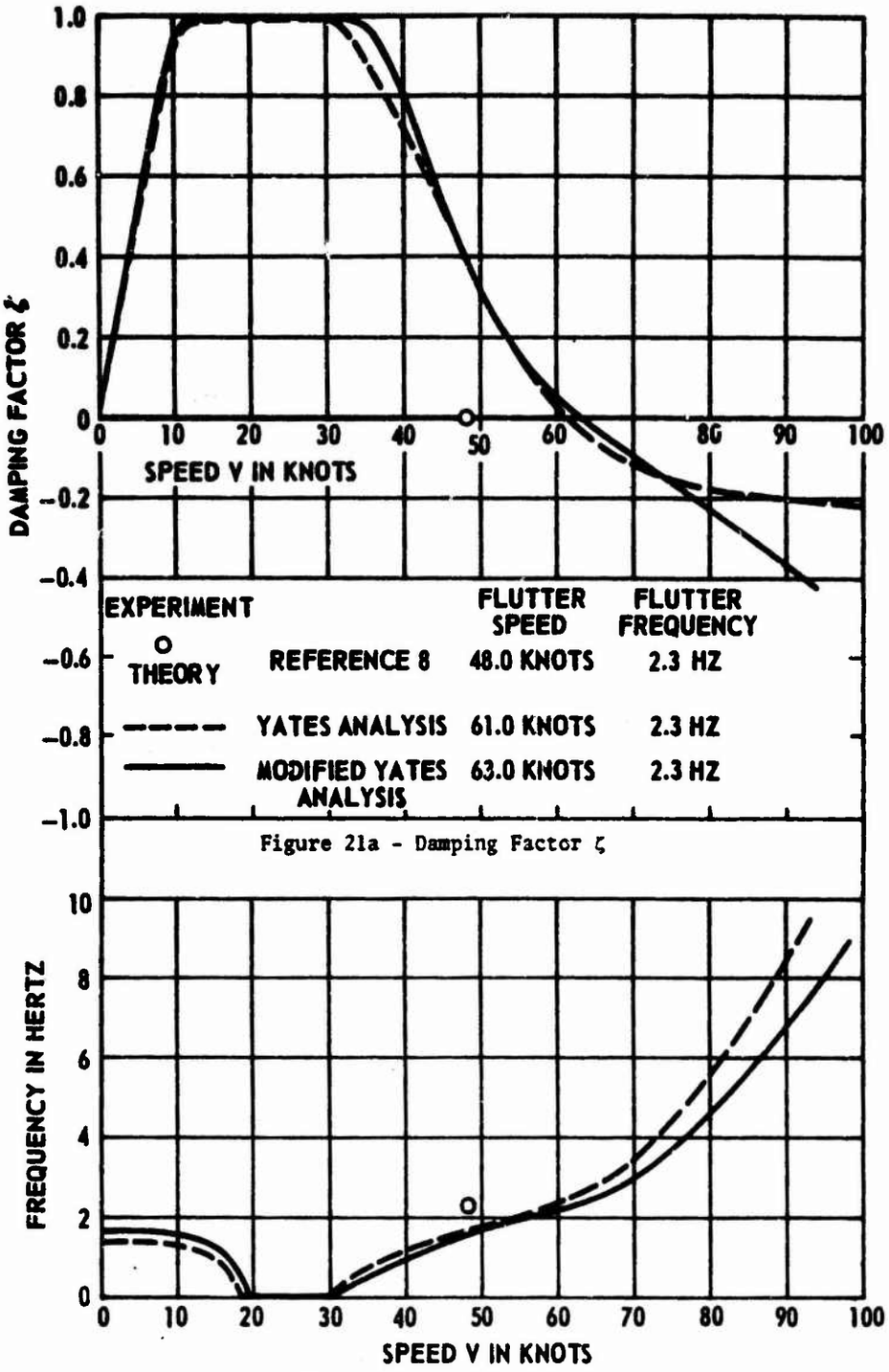

Figure 21a - Damping Factor ζ

Figure 21b - Frequency

Figure 21 - Critical Flutter Modes as Functions of Speed for Grumman Model 3

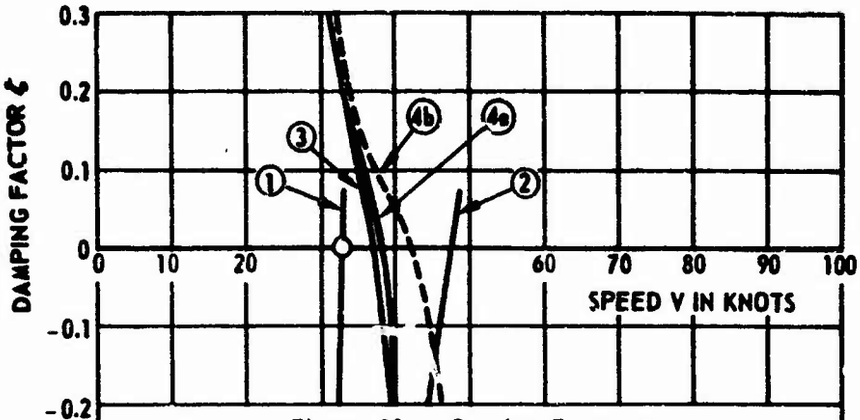

Figure 22a - Damping Factor ζ

EXPERIMENT		FLUTTER SPEED	FLUTTER FREQUENCY
O	REFERENCE 9	32.5 KNOTS	0.3 HZ
THEORY			
①	2-DIMENSIONAL THEODORSEN LOADING, MODAL ANALYSIS (REF. 3)	32.4 KNOTS	0.46 HZ
②	GENERALIZED LIFTING SURFACE THEORY (REF. 3)	47.2 KNOTS	0.73 HZ
③	YATES ANALYSIS	37.0 KNOTS	0.35 HZ
④	MODIFIED YATES ANALYSIS		
	(a) LOW-FREQUENCY SURFACE BOUNDARY CONDITION	38.0 KNOTS	0.65 HZ
	(b) HIGH-FREQUENCY SURFACE BOUNDARY CONDITION	42.0 KNOTS	0.5 HZ

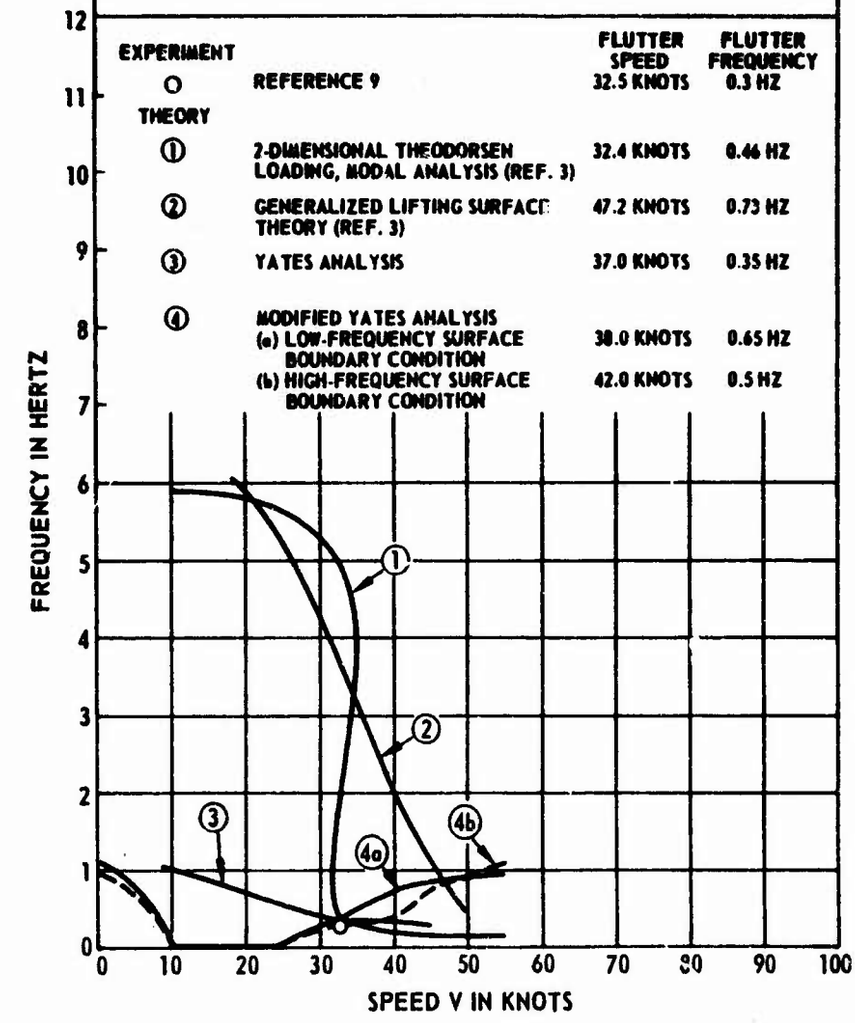

Figure 22b - Frequency

Figure 22 - Critical Flutter Modes as Functions of Speed for Grumman Model A

TABLE 1

Comparison of Analytical and Measured Natural Frequencies in Vacuum of SwRI 30-Inch Flutter Model

Mode Number	Measured in Air[4] Hz	Analytical in Vacuum Hz
1	9.63	10.1
2	31.9	28.3
3		50.2
4		79.4
5		116.7
6		126.4

TABLE 2

Comparison of Analytical and Measured Natural Frequencies in Water of SwRI 30-Inch Flutter Model

Mode Number	Measured[4] Hz	Analytical Hz
1	7.3	8.0
2	23.8	23.6
3		40.0
4		62.3
5		92.2
6		103.1

TABLE 3

Comparison of Analytical and Measured First Bending and First Torsional Mode Shapes in Vacuum of SwRI 30-Inch Flutter Model

	y/L	First Coupled Bending-Mode Shape Translational Deflection		First Coupled Torsional-Mode Shape Rotational Deflection	
		Measured in Air[4]	Analytical in Vacuum	Measured in Air[4]	Analytical in Vacuum
Root	0	0.	0.	0.	0.
	0.1	0.025	0.018	0.213	0.202
	0.2	0.075	0.065	0.403	0.393
	0.3	0.158	0.139	0.570	0.564
	0.4	0.260	0.232	0.710	0.708
	0.5	0.370	0.342	0.825	0.823
	0.6	0.488	0.464	0.915	0.905
	0.7	0.610	0.593	0.966	0.959
	0.8	0.738	0.727	0.990	0.988
	0.9	0.870	0.863	0.999	0.999
Tip	1.0	1.000	1.000	1.000	1.000

TABLE 4

Comparison of Analytical and Measured Natural Frequencies in Vacuum of Grumman Model 1

Mode Number	Measured in Air Hz		Analytical in Vacuum Hz	Mode Shape
	Ref. 8	Ref. 3		
1	2.87	2.83	2.88	1st Bending
2	18.2	18.00	17.43	2nd Bending
3	37.5	38.08	38.59	1st Torsion
4	49.7	49.92	46.70	3rd Bending
5	94.8	97.02	86.23	4th Bending
6	111.0	116.0	114.8	2nd Torsion

TABLE 5

Analytical Natural Frequencies in Water
of Grumman Model 1

Mode Number	Analytical in Water Hz	Mode Shape
1	1.38	1st Bending
2	8.39	2nd Bending
3	21.14	1st Torsion
4	23.39	3rd Bending
5	44.59	4th Bending
6	66.00	2nd Torsion

TABLE 6

Comparison of Analytical and Measured Natural Frequencies
in Vacuum of Grumman Model 2

Mode Number	Measured in Air[8] Hz	Analytical in Vacuum Hz	Predominant Mode Shape
1	4.90	4.82	1st Bending
2	29.8	29.03	2nd Bending
3	47.5	42.69	1st Torsion
4	80.82	77.18	3rd Bending
5	138.0	127.4	2nd Torsion
6	--	140.6	4th Bending

TABLE 7

Analytical Natural Frequencies in Water
of Grumman Model 2

Mode Number	Analytical in Water Hz	Predominant Mode Shape
1	2.58	1st Bending
2	15.61	2nd Bending
3	29.22	1st Torsion
4	43.72	3rd Bending
5	81.45	4th Bending
6	92.66	2nd Torsion

TABLE 8

Analytical Natural Frequencies in Vacuum
of Grumman Model 3

Mode Number	Analytical in Vacuum Hz	Predominent Mode Shape
1	4.75	1st Bending
2	28.59	2nd Bending
3	44.36	1st Torsion
4	76.02	3rd Bending
5	132.2	2nd Torsion
6	138.8	4th Bending

TABLE 9

Analytical Natural Frequencies in Water
of Grumman Model 3

Mode Number	Analytical in Water Hz	Predominant Mode Shape
1	1.65	1st Bending
2	10.06	2nd Bending
3	20.72	1st Torsion
4	28.48	3rd Bending
5	53.44	4th Bending
6	67.22	2nd Torsion

TABLE 10

Comparison of Analytical and Measured Natural Frequencies
in Vacuum of Grumman Model A

Mode Number	Measured in Air[3] Hz	Analytical in Vacuum Hz	Predominant Mode Shape
1	3.20	3.21	1st Bending
2	19.67	19.31	2nd Bending
3	32.45	33.90	1st Torsion
4	53.88	51.22	3rd Bending
5	107.0	92.85	4th Bending
6	100.7	101.5	2nd Torsion
7	--	140.2	5th Bending
8	164.9	166.9	3rd Torsion

TABLE 11

Analytical Natural Frequencies in Water
of Grumman Model A

Mode Number	Analytical in Water Hz	Predominent Mode Shape
1	1.11	1st Bending
2	6.47	2nd Bending
3	14.46	1st Torsion
4	17.19	3rd Bending
5	31.80	4th Bending
6	42.95	2nd Torsion
7	49.24	5th Bending
8	67.60	6th Bending

BLANK

APPENDIX

DESCRIPTION OF FLUTTER MODELS

SwRI 30-INCH MODEL

A detailed description of this model was given in Reference 4. The model consisted of a steel spar to which lead segments were attached. The planform and profile are shown in Figure 23, and the structural characteristics are summarized in Table 12. A reflecting plate was attached to the root of the model to eliminate the free surface effect.

GRUMMAN MODEL 1

This model was Grumman Model 1 of Reference 8. It was constructed of solid steel. The planform and profile are shown in Figure 24, and the structural characteristics are summarized in Table 13.

GRUMMAN MODELS 2 AND 3

These two models were Grumman Models 2 and 3 of Reference 8. Models 2 and 3 (Figure 25) are geometrically identical struts constructed of solid steel and solid aluminum respectively. Their structural characteristics are summarized in Tables 14 and 15.

GRUMMAN MODEL A

This model was Grumman Model A of Reference 9. The planform and profile are shown in Figure 26 and its structural characteristics are summarized in Table 16.

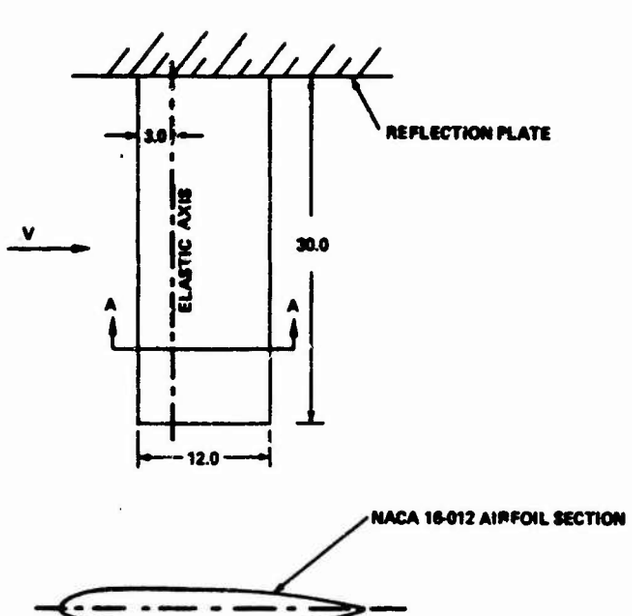

Figure 23 - SwRI 30-Inch Flutter Model

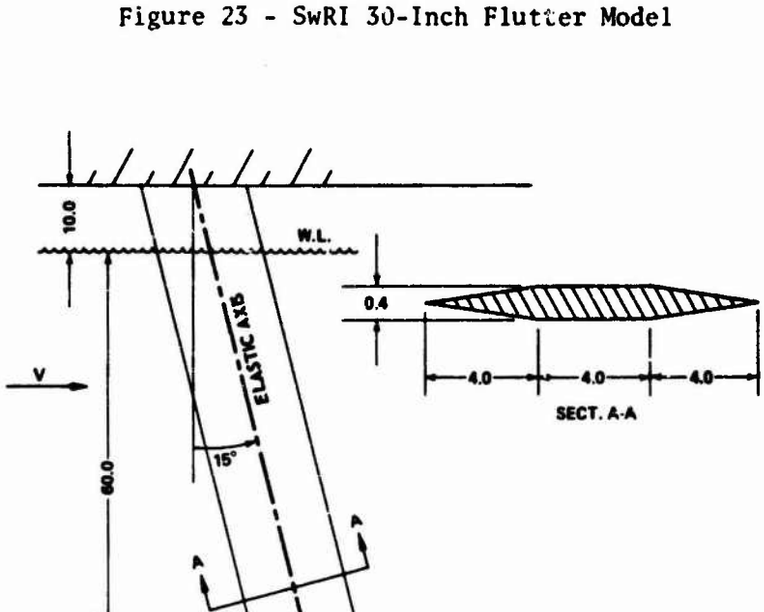

Figure 24 - Grumman Model 1

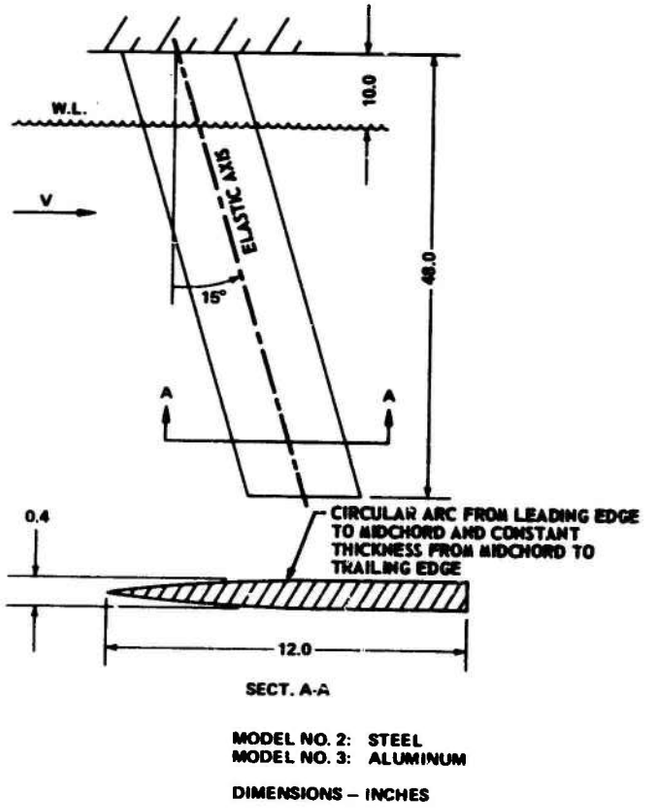

Figure 25 - Grumman Models 2 and 3

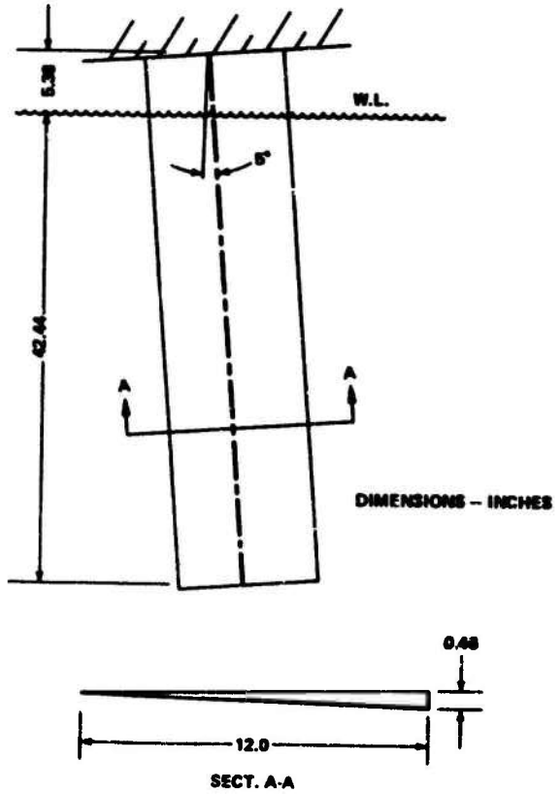

Figure 26 - Grumman Model A

TABLE 12

SwRI 30-Inch Flutter Model Structural Characteristics

Model Parameter	Measured Value
Aspect ratio AR	5.0
Semispan L in in.	30.0
Sweep angle Λ_{ea} in deg	0.0
Semichord b in in.	6.0
Mass per unit span m in lb-sec^2/in.^{2}	0.0105
Mass ratio μ	0.99
Elastic axis location a	-0.5
Center of gravity location x_α	0.524
Radius of gyration r_α^2	0.512
Bending stiffness EI in lb-in.^{2}	3.40×10^6
Torsional stiffness GJ in lb-in.^{2}	0.973×10^6
Total weight (wing only) in lb	121.2

TABLE 13

Grumman Model 1 Structural Characteristics

Model Parameter	Value
Aspect ratio AR	10.35
Semispan L in in.	62.1
Sweep angle Λ_{ea} in deg	15.0
Semichord b in in.	6.0
Mass per unit span m in lb-sec^2/in.^{2}	0.00232
Mass ratio μ	0.22
Elastic axis location a	0.0
Center of gravity location x_α	0.0
Radius of gyration r_α^2	0.1975
Bending stiffness EI* in lb-in.^{2}	0.9564×10^6
Torsional stiffness GJ* in lb-in.^{2}	1.555×10^6

*EI is 0.928×10^6 lb-in.^{2}. GJ is 1.52×10^6 lb-in.^{2} in Reference 3, in which results were obtained by calibrating after-flutter-tested model.

TABLE 14

Grumman Model 2 Structural Characteristics

Model Parameter	Value
Aspect ratio AR	8.57
Semispan L in in.	49.693
Sweep angle Λ_{ea} in deg	15
Semichord b in in.	5.796
Mass per unit span m in lb-sec^2/in.^{2}	0.00273
Mass ratio μ	0.28
Elastic axis location a	0.38
Center of gravity location x_α	-0.214
Radius of gyration r_α^2	0.358
Bending stiffness EI in lb-in.^{2}	1.293×10^6
Torsional stiffress GJ in lb-in.^{2}	2.070×10^6

TABLE 15

Grumman Model 3 Structural Characteristics

Model Parameter	Value
Aspect ratio AR	8.57
Semispan L in in.	49.693
Sweep angle Λ_{ea} in deg	15
Semichord b in in.	5.796
Mass per unit span m in lb-sec^2/in.^{2}	0.00094
Mass ratio μ	0.10
Elastic axis location a	0.38
Center of gravity location x_α	-0.214
Radius of gyration r_α^2	0.326
Bending stiffness EI in lb-in.^{2}	0.431×10^6
Torsional stiffness GJ in lb-in.^{2}	0.691×10^6

TABLE 16

Grumman Model A Structural Characteristics

Model Parameter	Value
Aspect ratio AR	8.251
Semispan L in in.	48
Sweep angle Λ_{ea} in deg	5
Semichord b in in.	6
Mass per unit span m in lb-sec^2/in.^{2}	0.00097475
Mass ratio μ	0.09
Elastic axis location a	-0.0784
Center of gravity location x_α	0.2724
Radius of gyration r_α^2	0.3254
Bending stiffness EI in lb-in.^{2}	0.174×10^6
Torsional stiffness GJ in lb-in.^{2}	0.370×10^6

REFERENCES

1. Henry, C. J., "Comparison of Hydrofoil Flutter Phenomenon and Airfoil Flutter Theory," Proceedings Fourth Naval Hydrodynamics Symposium (Aug 1962).

2. Cieslowski, D. S. and Besch, P. K., "Flutter of a Two-Degree-of-Freedom Hydrofoil in Two-Dimensional Subcavitating Flow," NSRDC Report 3183 (Jan 1970).

3. Rowe, W. S. and Marvin, T. G. B., "A Program of Theoretical Research on Hydroelastic Stability," The Boeing Company, Contract N00014-67-C-0248 (Nov 1968).

4. Abramson, H. N. and Langner, C. G., "Correlation of Various Subcavitating Hydrofoil Flutter Predictions Using Modified Oscillatory Lift and Moment Coefficients," Contract NObs-88599, Southwest Research Institute (Jun 1964).

5. Yates, E. C., Jr., "Flutter Prediction at Low Mass-Density Ratios with Application to the Finite-Span Noncavitating Hydrofoil," AIAA Third Marine Systems and ASW Meeting (Apr-May 1968).

6. Yates, E. C., Jr., "Calculation of Flutter Characteristics for Finite-Span Swept or Unswept Wings at Subsonic and Supersonic Speeds by a Modified Strip Analysis," NACA RM L57L10 (1958).

7. Widnall, S. E., "Unsteady Loads on Hydrofoils Including Free Surface Effects and Cavitation," Massachusetts Institute of Technology, Fluid Dynamics Research Laboratory Report No. 64-2 (Jun 1964).

8. Baird, E. F. et al., "Investigation of Hydrofoil Flutter," Report No. DA 10-480.3, Grumman Aircraft Engineering Corporation (Feb 1962).

9. Squires, C. E., Jr., "Hydrofoil Flutter Small Sweep Angle Investigation Final Report," Report No. DA Nonr-3938.3, Grumman Aircraft Engineering Corporation (Nov 1963).

10. Leibowitz, R. C. and Kennard, E. H., "Theory or Freely Vibrating Nonuniform Methods of Solution and Application to Ships," DTMB Report 1317 (May 1961).

11. Peterson, L., "SADSAM V User's Manual," MacNeal-Schwendler Corporation Project Report (Dec 1970).

12. Theodorsen, T., "General Theory of Aerodynamic Instability and the Mechanism of Flutter," NACA Report 496 (1935).